# Supporting Information for

# "Topographical and compositional engineering of core-shell Ni@Pt ORR electro-catalysts"

Gerard M. Leteba,[a,b] David R.G. Mitchell,[c] Pieter B.J. Levecque,[a] Eric van Steen[a] and Candace I. Lang[b]*

[a] Catalysis Institute, Department of Chemical Engineering, University of Cape Town, Cape Town 7700, South Africa
[b] School of Engineering, Macquarie University, Sydney NSW 2109, Australia
[c] Electron Microscopy Centre, Innovation Campus, University of Wollongong, Wollongong NSW 2517, Australia

*Corresponding author: Candace I. Lang

E-mail: *candace.lang@mq.edu.au

## Experimental Sections

**Chemicals and materials.** The synthetic method employed the following metal precursors (Sigma-Aldrich): chloroplatinic acid solution ($H_2PtCl_6$, 8 wt. % in water), platinum acetylacetonate ($Pt(acac)_2$, 97%) and nickel (II) acetate tetrahydrate ($Ni(Ac)_2{\cdot}4H_2O$, ≥98%). Oleylamine (OAm, ≥98%), octadecylamine (ODA, 90%) and oleyl alcohol (OA, 85%) were employed as surfactants and 1-octadecene (1-ODE, 90%), as a high-boiling point solvent. Tetrabutylammonium borohydride (TBAB, 98%) was used as a reducing agent. Carbon black (Vulcan XC-72R) was used to support the as-synthesised nanoparticles. Isopropanol (≥99.5%) and Nafion® perfluorinated resin solution (5 wt. % in a mixture of lower aliphatic alcohols and water (45% water)), were employed to formulate the catalyst ink. Perchloric acid ($HClO_4$, 70%) was used for electrochemical measurements. Solvents (Sigma-Aldrich) such as absolute ethanol, acetone and chloroform, used for precipitating, cleaning and re-dispersing the particles, were all of analytical grade. All the chemicals were used as-received without any further purification.

## Simultaneous Reduction by Thermolysis

(a) In a typical reduction method: $Ni(Ac)_2{\cdot}4H_2O$ (0.24 mmol) and dried $H_2PtCl_6$ (8 wt.% in $H_20$, 0.82 mmol) precursor salts dissolved in 15 ml OAm and 4.4 g ODA (surfactants) in a high-boiling point, 20 ml 1-OD, followed by sonication for 20 minutes. The resultant mixture was rapidly heated to 310 °C for 30–40 minutes. The reduction of the metal precursor salts was influenced by both the reduction temperature and the surfactants. Upon reduction, the synthesis solution turned from deep green to dark black, forming dense precipitates. The synthesis organic medium was removed from the heat source and allowed to cool down to room temperature. The black nanoparticle products collected at the bottom of the round-bottom flask were purified by the addition of excess ethanol. After complete settling (typically overnight), the excess organic solvents were decanted and the particles were further cleaned by re-suspending in ethanol/acetone mixture of equal volumes. This process was repeated 5 times. The black products were finally re-dispersed in 20 ml chloroform, yielding a dark black colloidal suspension.

A similar protocol was deployed to form binary PtNi nanoparticles but in the presence of oleyl alcohol (OA, 5 ml) as an additional surfactant. The precipitation-purification approach is similar to the one described above in (a).

(b) In a typical sequential reduction method: $Ni(Ac)_2{\cdot}4H_2O$ (0.24 mmol) and platinum acetylacetonate ($Pt(acac)_2$, 0.82 mmol) precursor salts were added and the solution was rapidly heated to 310 °C for 30–40 minutes. Upon reduction, the synthesis solution turned from deep green to dark black, forming dense precipitates. The synthesis organic medium was removed from the heat source and allowed to cool down to room temperature. The black nanoparticle products collected at the bottom of the round-bottom flask were purified by the addition of excess ethanol. After complete settling (typically overnight), the excess organic solvents were decanted and the particles were further cleaned by re-suspending in ethanol/acetone mixture of equal volumes. This process was repeated 5 times. The black products were finally re-dispersed in 20 ml chloroform, yielding a dark black colloidal suspension.

A similar protocol was deployed to form binary PtNi nanoparticles but in the presence of OA as third surfactant component. The purification approach is similar to the one described above in (a) and (b).

(c) The synthesis approaches reported in sections (a) and (b) were used to prepare PtNi nanoparticles with the inclusion of tetrabutylammonium borohydride (TBAB) as a reducing agent. The difference here is that the synthesis mixtures turned from deep green to dark brown and there was no significant formation of dense precipitates. The precipitation-purification approaches are similar to the ones described above in (a), (b) and (c).

**Nanostructure characterization techniques.** The black powders of the as-synthesised nanostructures were deposited onto a zero-background silicon (Si) wafer support and characterized by powder XRD on an X'Pert Pro multipurpose diffractometer (MPD), using Cu $K_\alpha$ radiation ($\lambda$ = 0.154056 nm). The diffraction patterns were recorded at a scan rate of 0.106º/s and with a step size of 0.0334º. Specimens for scanning transmission electron microscopy (STEM) investigations were prepared by drop-casting a colloidal solution onto 3-mm carbon-supported films on copper grids. These were air dried under ambient conditions. Specimens were analysed using TEM, HRTEM and STEM on a JEOL ARM200F probe-corrected instrument, operating at 200 kV. The chemical compositions of individual nanoparticles were determined using energy dispersive X-ray spectroscopy (EDS) in STEM mode. Spectrum imaging was used in which an EDS spectrum is obtained at each pixel in the STEM Image, to produce a 3D dataset. Rapid acquisition was used (5s per frame) integrated over at least 100 frames. Image drift correction was applied after each frame. Scanning TEM (STEM) imaging used bright field and high angle annular dark field (HAADF) imaging modes.

**Deposition of nanomaterials onto carbon support.** The as-prepared nanostructures were dispersed onto a carbon support (Cabot, Vulcan XC-72R) via a colloidal-deposition strategy, by mixing these nanomaterials and chloroform, followed by sonication for 15 min. The resulting homogeneous reaction dispersion was left in a fume hood for 5 hours to evaporate the chloroform. The resultant carbon-supported materials were further washed with acetone 5 times and dried in an oven at 60 ºC. The metal loading (wt.% metal) for each sample was verified using thermogravimetric analysis (Mettler Toledo TGA/sDTA851e).

**Electrochemical Measurements.** All experiments were performed in a standard three electrode setup at room temperature in a 0.1 M perchloric acid ($HClO_4$, 70%) solution using either argon (Ar) 99.999% (Afrox), oxygen ($O_2$) 99.998% (Afrox) and carbon dioxide (CO) 99% (Afrox) as specified. A platinum (Pt) coil was used as the counter electrode. A mercury/mercurous sulphate reference electrode was used as a reference and all potential values were reported relative to the standard hydrogen electrode (SHE). The readout currents were not corrected for the ohmic iR losses. A Biologic SP300 potentiostat was coupled to a RDE710 Rotator (Gamry instrument). Catalyst inks were prepared by mixing 10 mg of the catalyst with 2 ml of Milli-Q water (Millipore, 18 MΩ.cm @ 25 °C), 0.45 ml isopropanol and 25 µl Nafion® perfluorinated resin solution (5 wt.% in a mixture of lower aliphatic alcohols and water (45% water)). The resultant mixture was sonicated for 15 min. 10 µl of the ink was then pipetted onto a glassy carbon (GC) electrode (Pine Research Instrumentation, 5 mm disk OD) and dried under ambient conditions for 60 min to evaporate the solvents. The remaining thin black uniform film of Nafion-catalyst-Vulcan on the GC served as the working electrode (WE). Before use the GC electrode was polished to a mirror finish on a Microcloth polishing pad (Buehler) using 1 µm and 0.05 µm alumina paste (Buehler). After rinsing, the WE was ultrasonicated in Milli-Q water (Millipore, 18 MΩ.cm @ 25 °C) for 10–15 min and left to dry.

(a) **Cyclic voltammetry.** In an Ar purged electrolyte, the potential of the WE was cycled between 0.05 V and 1.00 V vs. SHE at a scan rate of 100 mV/s for 100 cycles to electrochemically clean the catalyst surface. The

sweep rate was then reduced to 50 mV/s and the third cycle at that scan rate was used for analysis. The electrochemically active surface area (ECSA) was calculated by integrating the area under the curve for the hydrogen underpotential deposition region ($H_{upd}$) assuming a monolayer hydrogen charge of 210 $\mu C/cm^2_{Pt.}$[1,2]

(b) **Carbon dioxide (CO) stripping voltammetry.** CO gas was bubbled into the electrolyte solution while holding the potential of the working electrode at 0.1 V vs. SHE. The electrolyte was then purged with Ar to remove the dissolved CO gas while still holding the potential of the WE at 0.1 V vs. SHE. The potential of the WE was then cycled to 1.00 V vs. SHE at 20 mV/s, followed by a CV cycle as described above at 20 mV/s. The peak area could then be determined using the baseline CV and a normalisation factor of 420 $\mu g/cm^2_{Pt}$[3] was used to calculate the ECSA.

(c) **Linear Sweep Voltammetry.** The potential of the WE was swept from 1.10 V to 0.20 V vs. SHE and back at 10 mV/s. ORR polarization curves were recorded at rotation speeds of 400, 900, 1600 and 2500 rpm. The ORR curves obtained in $O_2$ saturated electrolyte were corrected for the capacitive current associated with $Pt_xM_y/C$ catalysts, by subtracting a CV curve measured in an argon-saturated electrolyte. All the polarization curves reported in this work were acquired using a rotation speed of 1600 rpm and the current densities were also normalized with reference to the calculated ECSA to evaluate the specific activities.

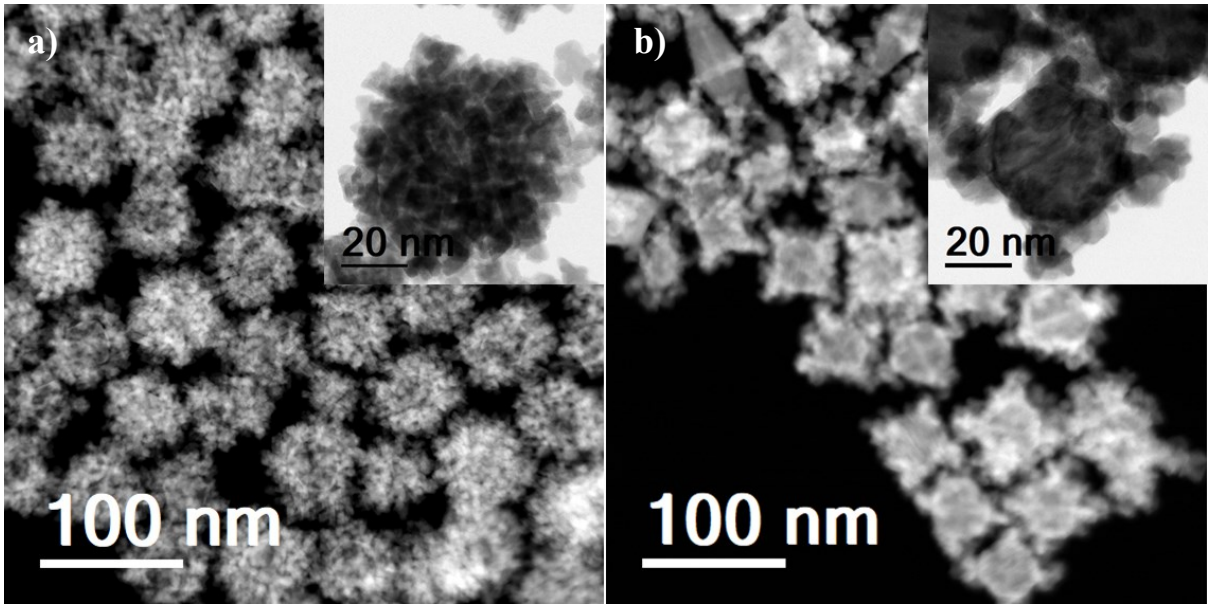


**Fig. S1** HAADF-STEM images of (a) PtNi(#1) and (b) PtNi(#2) nanoparticle populations showing bright Pt-rich heteroepitaxial growth configurations. Inset is the associated enlarged STEM bright field micrographs of these binary nanoparticles.

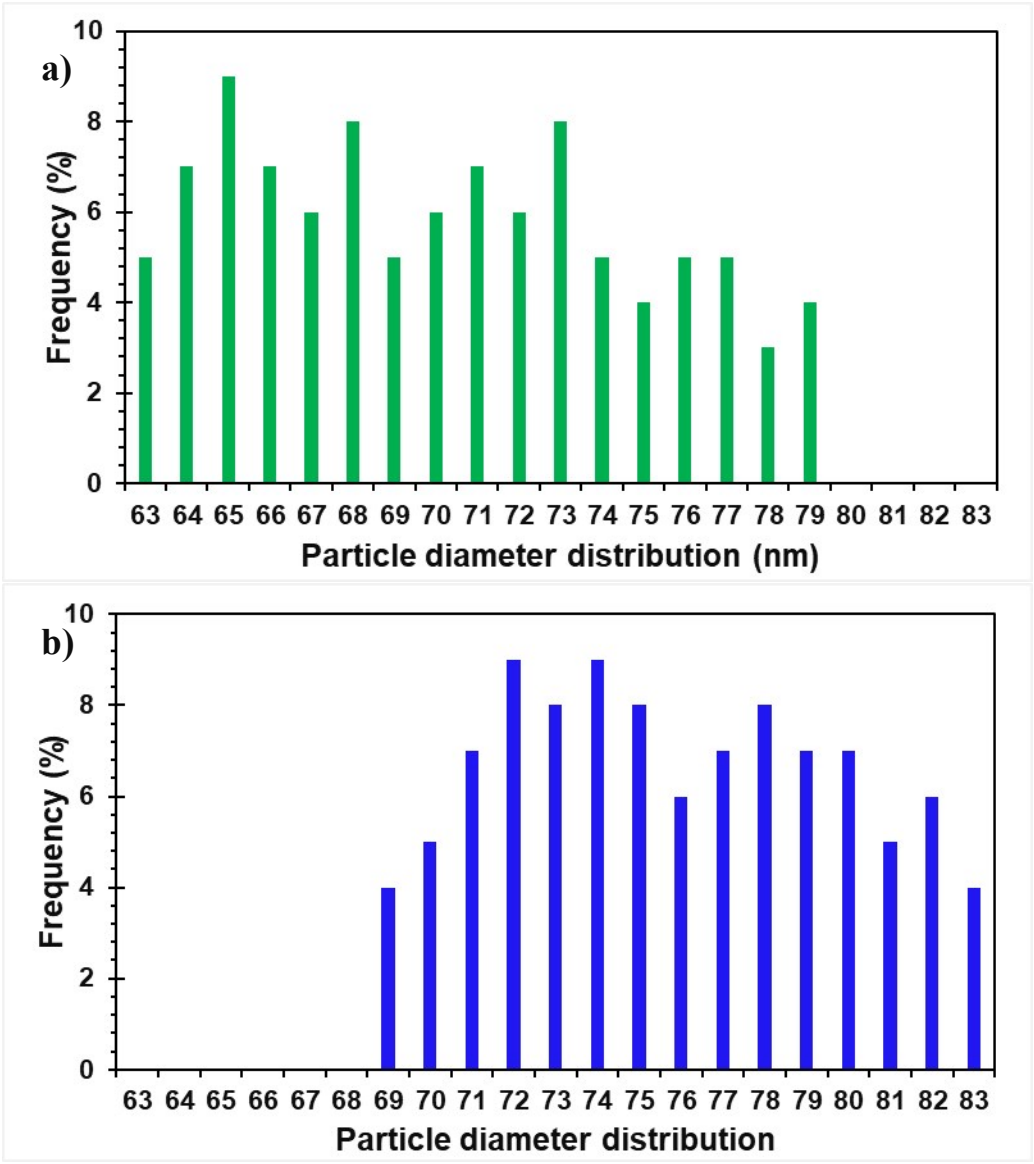


**Fig. S2** Particle size distribution (nm) histograms of binary (a) PtNi(#1) and (b) PtNi(#2) alloy nanoparticles.

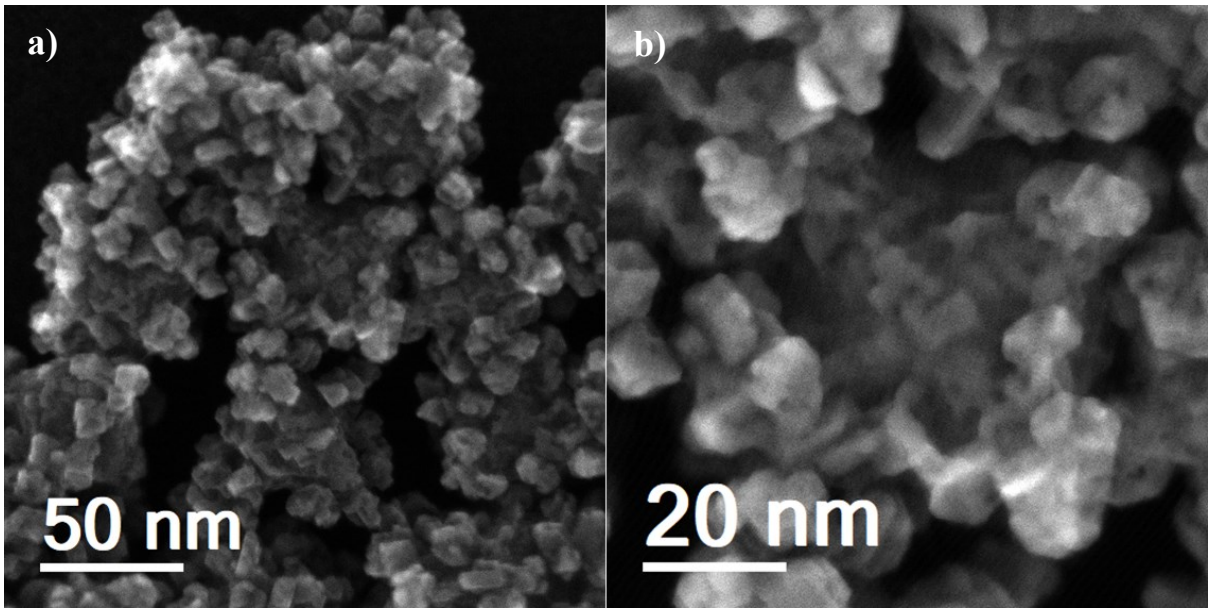


**Fig. S3** (a) Low magnification SE-STEM image revealing the surface topographic contrast of binary PtNi(#2) nanoparticles. (b) Detail of a)

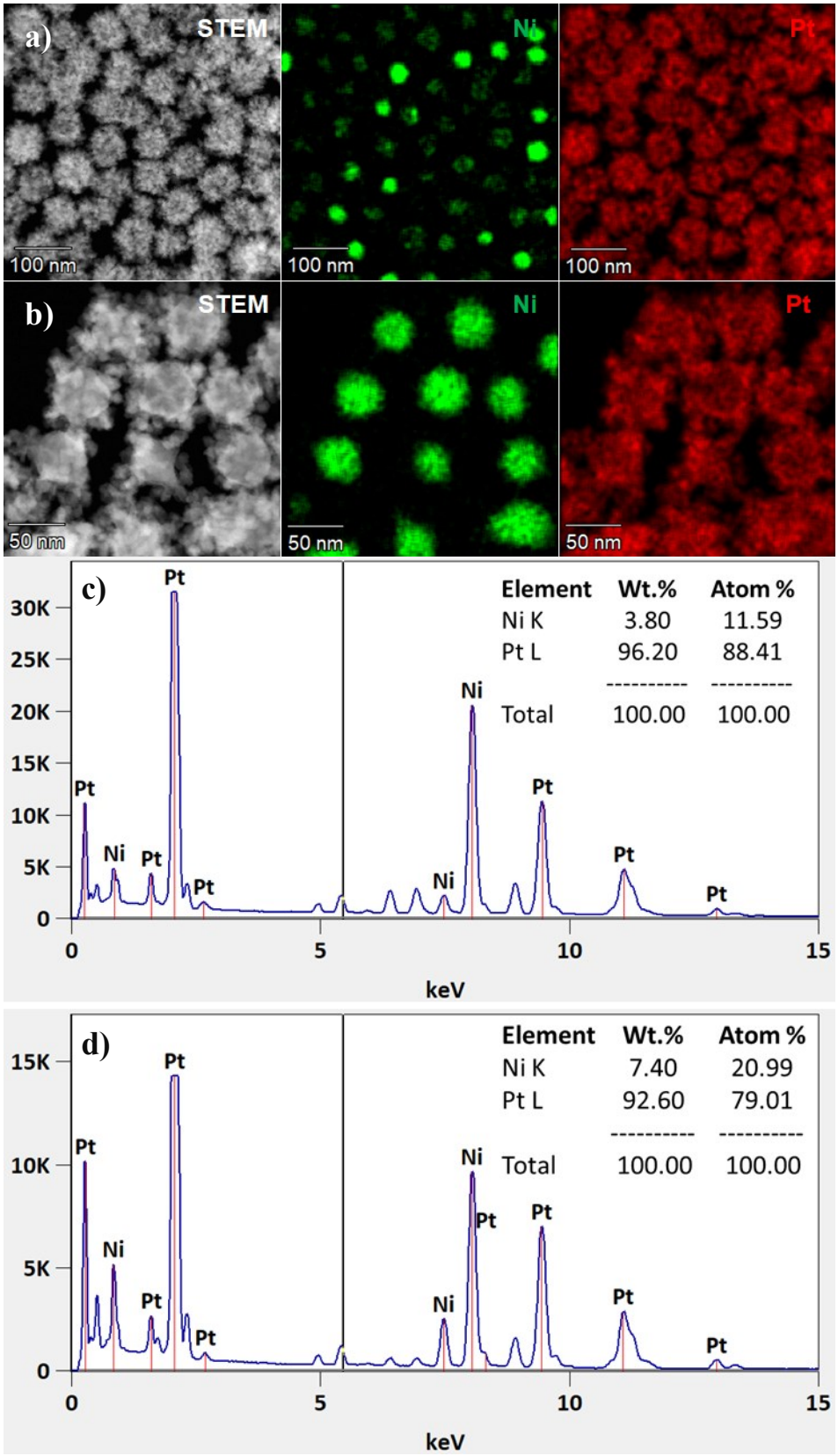


**Fig. S4** STEM-EDS elemental mapping for binary (a) PtNi(#1,S) and (b) PtNi(#2,C) alloy nanoparticles, revealing elemental distribution within single crystalline particles. (Left to right) (a) and (b)) HAADF-STEM micrographs, Ni (Kα) map (green) and Pt (Lα) map (red). The EDS maps show Ni core–Pt shell (Ni@Pt) structures. Average EDS spectra from these binary (c) PtNi(#1,S) and (d) PtNi(#2,C) alloy nanoparticles.

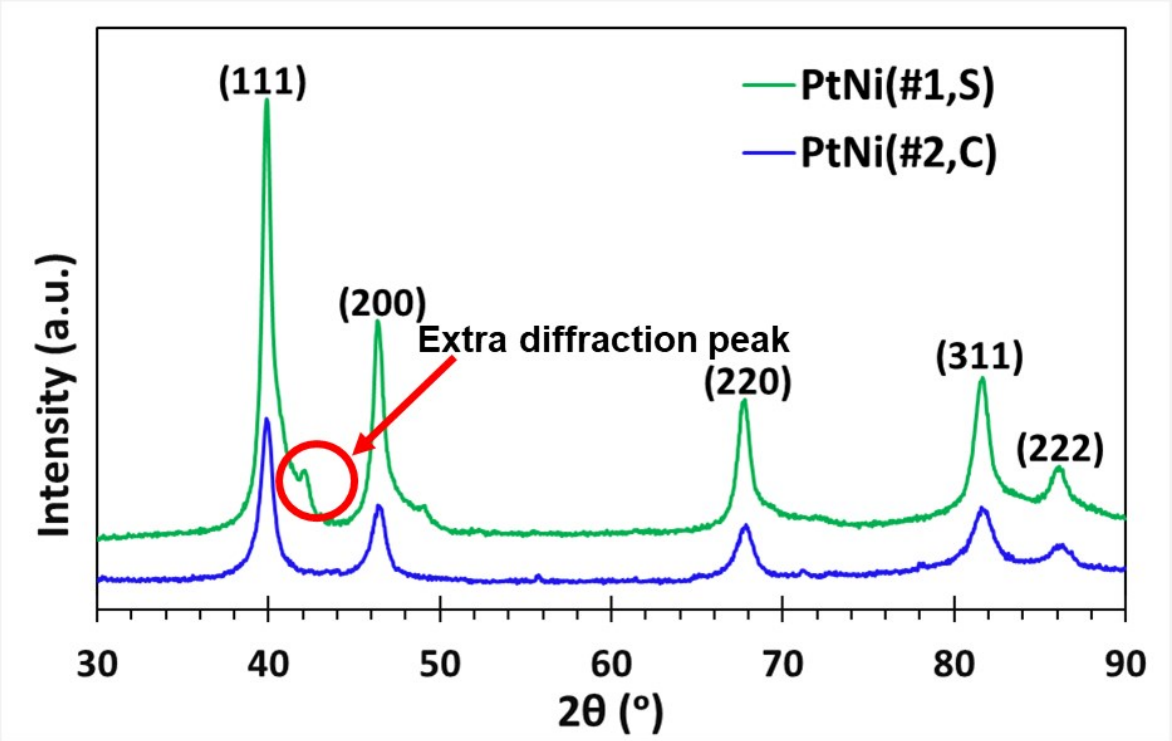


**Fig. S5** XRD patterns of PtNi(#1,S) and PtNi(#2,C) binary nanoparticles which are fcc.

## Lattice constants

$a_c = d_{hkl}(h^2 + k^2 + l^2)^{1/2}$ where $d_{hkl} = d_{111}$.

(a) **PtNi(#1)**

**Peak 1:** $a_c = d_{hkl}(3)^{1/2} = 0.225(3)^{1/2} = 0.390$ nm

**Peak 2:** $a_c = d_{hkl}(3)^{1/2} = 0.216(3)^{1/2} = 0.372$ nm

(b) **PtNi(#2)**

$a_c = d_{hkl}(3)^{1/2} = 0.221(3)^{1/2} = 0.383$ nm

## Vegard's Law

The expression for Vegard's law[4,5] for a binary solid solution A-B is:

$$d_{alloy} = Xd_A + (1 - X)Xd_B$$

where $X = XB$ is the mole fraction of component $B$, $Xd_A$ and $Xd_B$ are the lattice constants of pure components $A$ and $B$, respectively.

**Binary solid solution compositions from calculations using Vegard's rule:**

(a) **PtNi(#1)**

**Peak 1:** Lattice constant = 0.390 nm

**Pt**: $0.390 = 0.393(X) + (1 - X)0.352$

$X = 92.7\ at.\%$

**Ni**: $0.390 = 0.352(X) + (1 - X)0.393$

$X = 7.3\ at.\%$

**Peak 2:** Lattice constant = 0.372 nm

**Pt**: $0.372 = 0.393(X) + (1 - X)0.352$

$X = 48.8\ at.\%$

**Ni**: $0.372 = 0.352(X) + (1 - X)0.393$

$X = 51.2\ at.\%$

(b) **PtNi(#2):**

Lattice constant = 0.383 nm

**Pt**: $0.383 = 0.393(X) + (1 - X)0.352$

$X = 75.6\ at.\%$

**Ni**: $0.383 = 0.352(X) + (1 - X)0.393$

$X = 24.4\ at.\%$

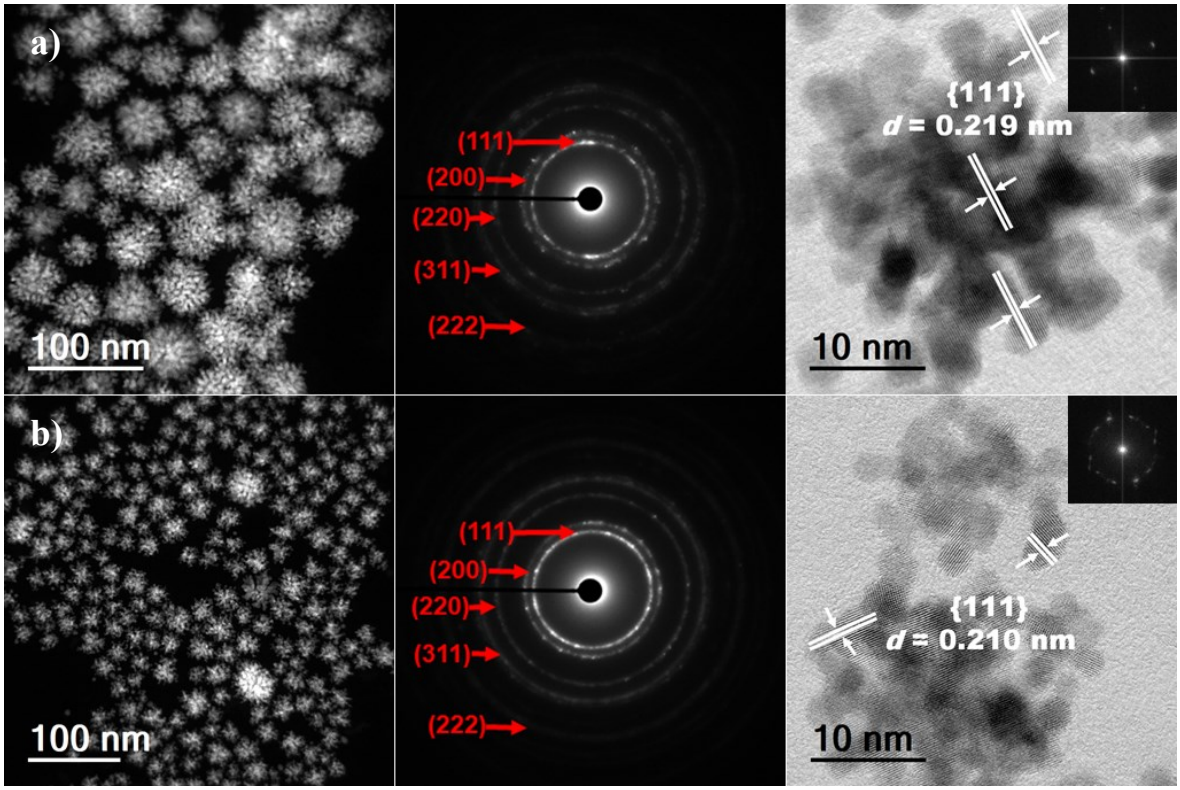


**Fig. S6** HAADF-STEM images of binary (a) PtNi(#3) and (b) PtNi(#4) alloy nanoparticles, the corresponding selected area electron diffraction patterns (centre - the planes assigned as indicated) and BF-STEM micrographs (right) of these particles (insert is FFT diffractogram) are shown.

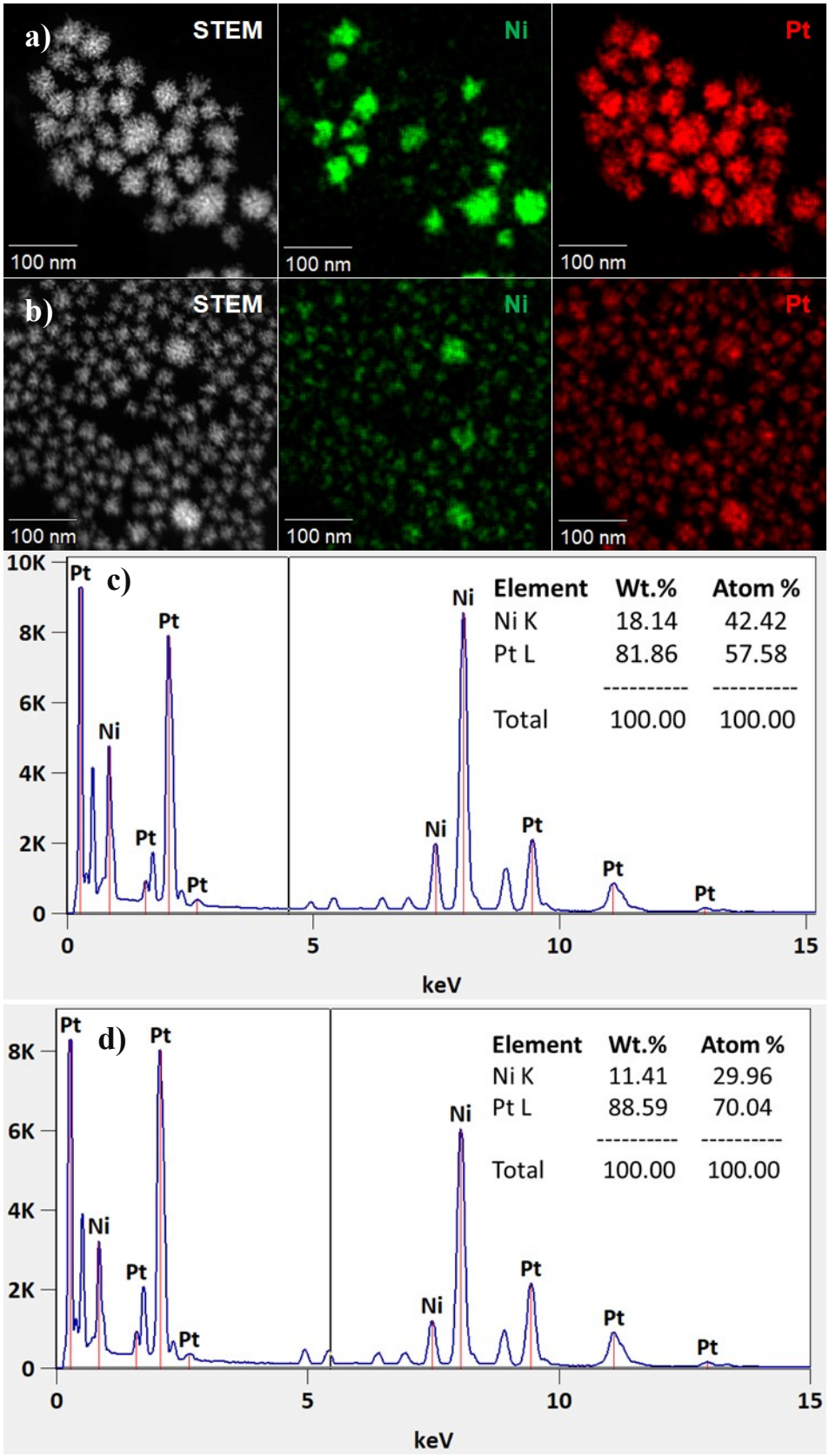


**Fig. S7** HAADF-STEM-EDS elemental mapping for binary (a) PtNi(#3) and (b) PtNi(#4) alloy nanoparticles, showing the elemental distributions within single crystalline particles. (Left to right) (a) and (b)) HAADF-STEM micrographs, Ni (Kα) map (green) and Pt (Lα) map (red). (c) and (d) are the corresponding average EDS maps showing core-shell Ni@Pt structures.

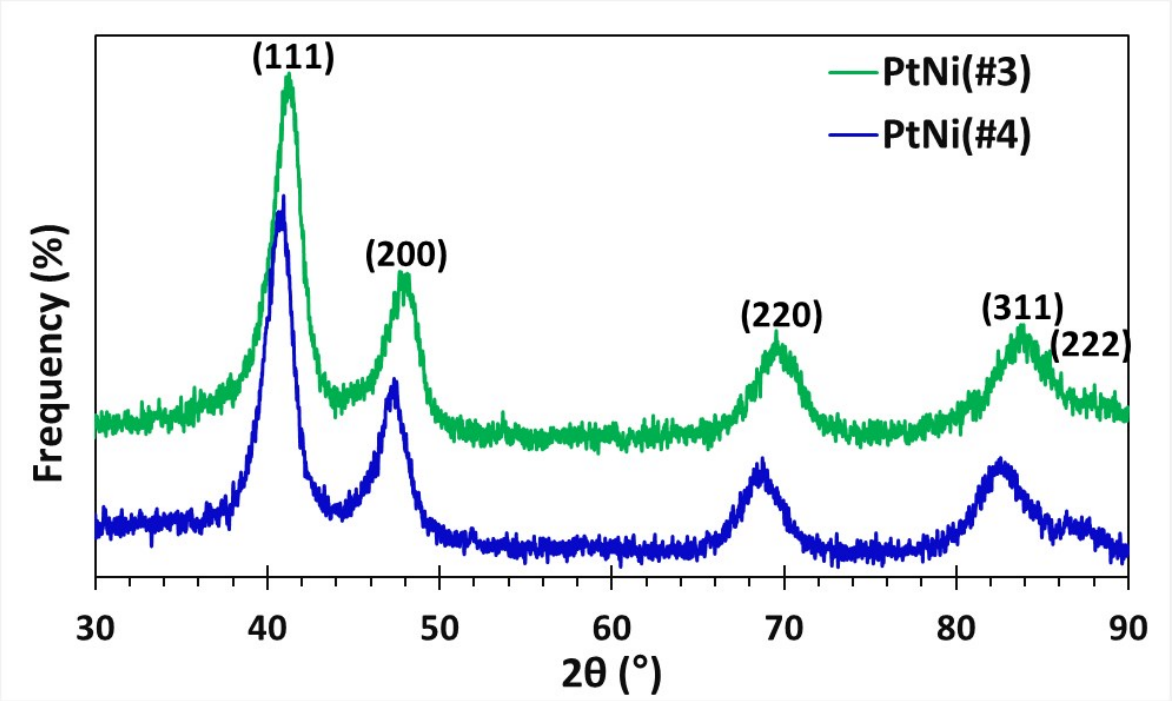


**Fig. S8** PXRD patterns of these PtNi(#3) and PtNi(#4) binary nanoparticles displaying fcc solid solution phases.

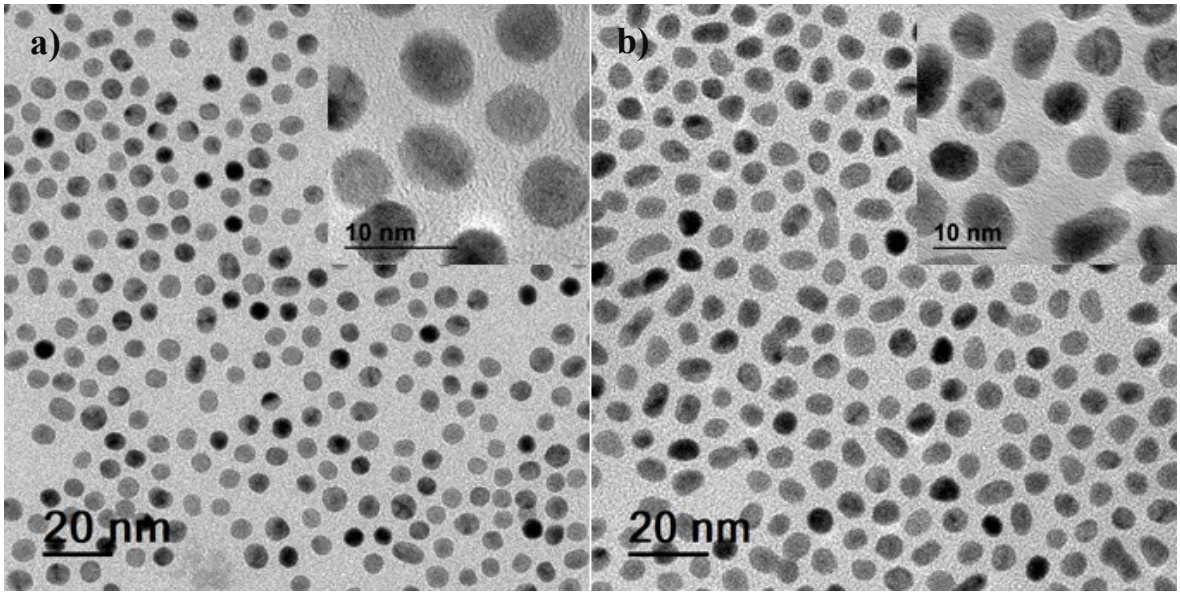


**Fig. S9** BF-TEM images of (a) PtNi(#6) and (b) PtNi(#8) NPs synthesized by co-reducing: $Ni(Ac)_2{\cdot}4H_2O$ and $H_2PtCl_6$; $Ni(Ac)_2{\cdot}4H_2O$ and $Pt(acac)_2$ precursors, respectively, using TBAB as a reductant in ternary surfactants (OAm, ODA and OA). Inserts are enlarged BF-STEM images.

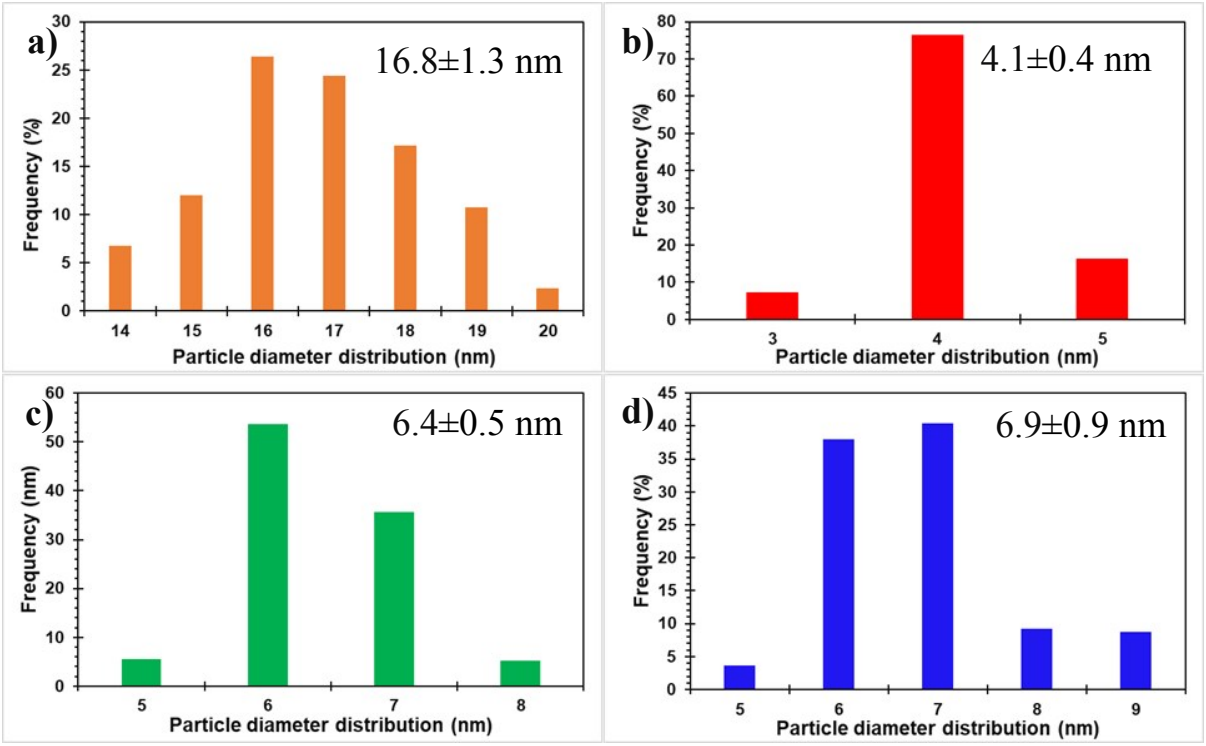


**Fig. S10** Particle size distributions of binary (a) PtNi(#5) and (b) PtNi(#6) alloy nanoparticles formed by co-reducing $Ni(Ac)_2{\cdot}4H_2O$ and $H_2PtCl_6$ precursors using tetrabutylammonium borohydride (TBAB). Particle size distribution histograms of (c) PtNi(#7) and (d) PtNi(#8) alloy particles prepared via co-reduction of $Ni(Ac)_2{\cdot}4H_2O$ and $Pt(acac)_2$ precursors using TBAB.

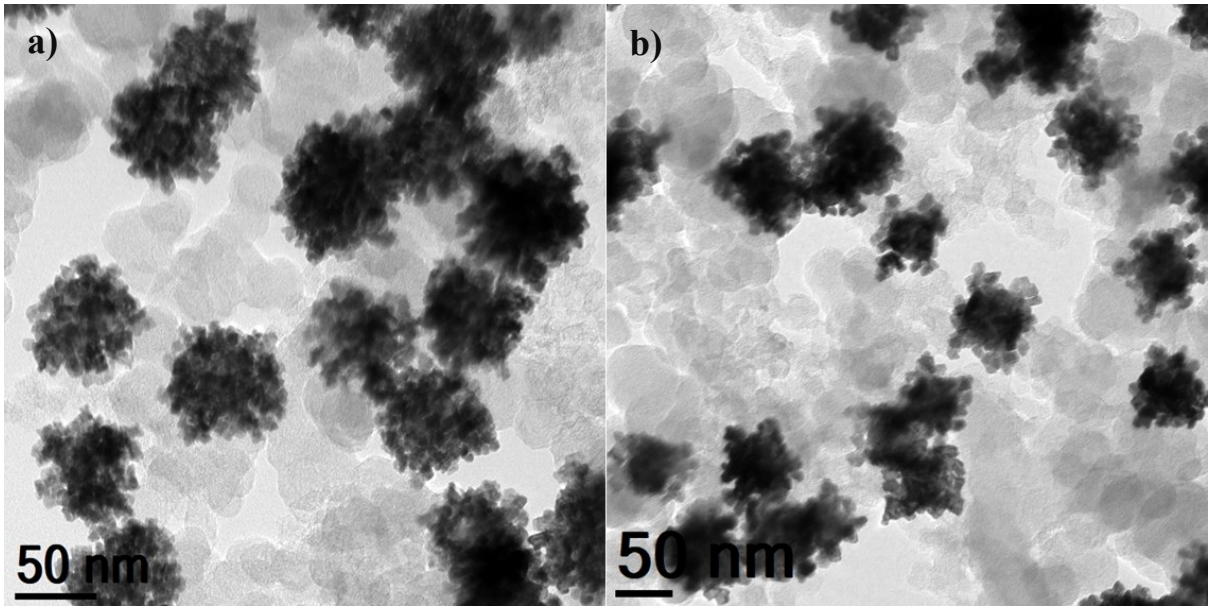


**Fig. S11** BF-TEM micrographs of (a) PtNi(#1,S) and (b) PtNi(#2,C) nanoparticles supported on high surface area carbon (Vulcan XC-72R).

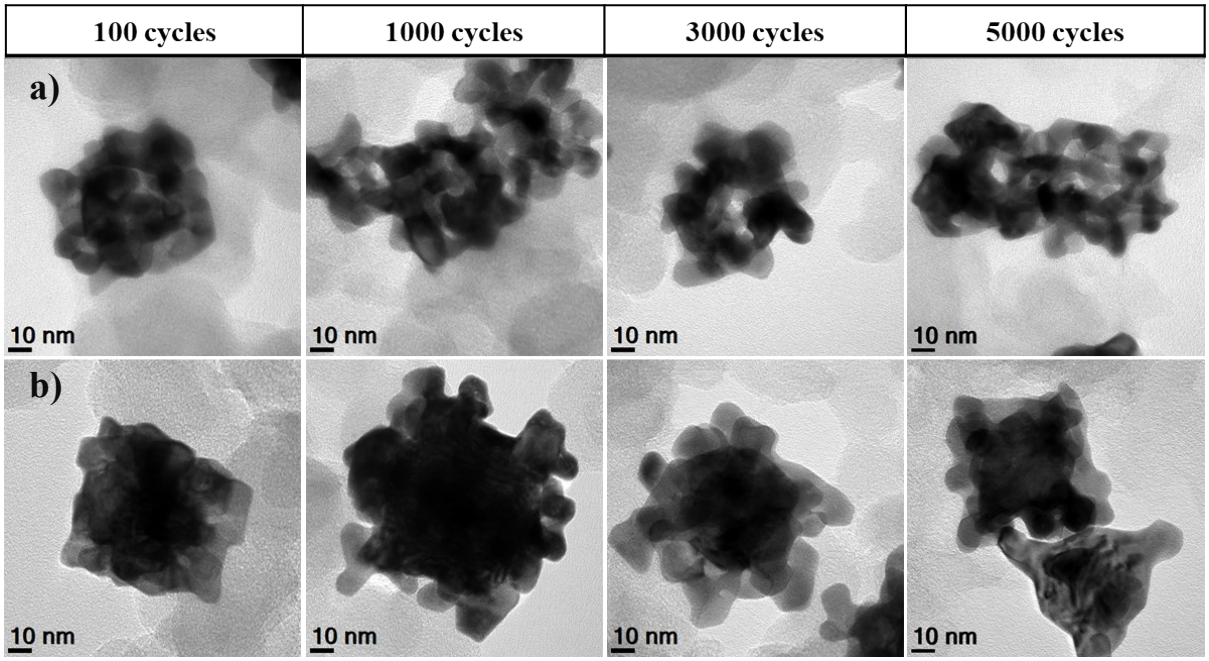


**Fig. S12** Representative BF-TEM micrographs of binary (a) PtNi(#1,S)/C and (b) PtNi(#2,C)/C materials showing microstructural change as a function of electrochemical cycling, up to 5000 cycles.

**Table S1** Summary of the activities of two types of binary electrocatalysts before and post 5000 extended electrochemical cycles: $ESCA_{Hupd}$, $ECSA_{CO}$, mass and specific activities of these core-shell Ni@Pt nanostructures.

| Catalysts | ECSA ($m^2/g_{Pt}$) (CV) | ECSA ($m^2/g_{Pt}$) loss (%) | ECSA ($m^2/g_{Pt}$) (CO stripping) | ECSA ($m^2/g_{Pt}$) (CO stripping) loss (%) | Mass activity ($A/mg_{Pt}$) | Mass activity loss (%) | Specific activity ($mA/cm^2_{Pt}$) | Specific activity loss (%) |
|---|---|---|---|---|---|---|---|---|
| PtNi(#1,S)/C | 0.1k cycles: 69.5 | | 0.1k cycles: 67.2 | | 0.33 | | 0.48 | |
| | 5k cycles: 23.8 | 66 | 5k cycles: 21.9 | 67 | 0.16 | 52 | 0.27 | 44 |
| PtNi(#2,C)/C | 0.1k cycles: 78.4 | | 0.1k cycles: 80.3 | | 0.42 | | 0.54 | |
| | 5k cycles: 64.1 | 18 | 5k cycles: 61.7 | 23 | 0.18 | 58 | 0.12 | 77 |

**Table S2** The ratio determined between $ECSA_{CO}$ and $ECSA_{Hupd}$ for PtNi(#1,S)/C and PtNi(#2,C)/C electrocatalysts before (0.1k cycles) and post extended electrochemical measurements (5k cycles).

| ECSA ($CO_{ad}$)/ECSA ($H_{upd}$) | PtNi(#1,S)/C | PtNi(#2,C)/C |
|---|---|---|
| 0.1k cycles | 0.97 | 1.02 |
| 5k cycles | 0.92 | 0.96 |

## References


1 T. R. Ralph, G. A. Hards, J. E. Keating, S. A. Campbell, D. P. Wilkinson, M. Davis, J. St-Pierre and M. C. Johnson, *J. Electrochem. Soc.* , 1997, **144**, 3845–3857.

2 J. I. Shui, C. Chen and J. C. M. Li, *Adv. Funct. Mater.*, 2011, **21**, 3357–3362.

3 F. Maillard, S. Schreier, M. Hanzlik, E. R. Savinova, S. Weinkauf and U. Stimming, *Phys. Chem. Chem. Phys.*, 2005, **7**, 385–393.

4 L. Vegard, *Zeitschrift für Phys.*, 1921, **5**, 17–26.

5 A. R. Denton and N. W. Ashcroft, *Phys. Rev. A*, 1991, **43**, 3161–3164.